

Simulations corroborate telegraph model predictions for the extension distributions of nanochannel confined DNA

Cite as: Biomicrofluidics 13, 044110 (2019); doi: 10.1063/1.5109566

Submitted: 9 May 2019 · Accepted: 21 July 2019 ·

Published Online: 8 August 2019



View Online



Export Citation



CrossMark

Aditya Bikram Bhandari and Kevin D. Dorfman^{a)} 

AFFILIATIONS

Department of Chemical Engineering and Materials Science, University of Minnesota—Twin Cities, 421 Washington Ave. SE, Minneapolis, Minnesota 55455, USA

^{a)}Electronic mail: dorfman@umn.edu

ABSTRACT

Hairpins in the conformation of DNA confined in nanochannels close to their persistence length cause the distribution of their fractional extensions to be heavily left skewed. A recent theory rationalizes these skewed distributions using a correlated telegraph process, which can be solved exactly in the asymptotic limit of small but frequent hairpin formation. Pruned-enriched Rosenbluth method simulations of the fractional extension distribution for a channel-confined wormlike chain confirm the predictions of the telegraph model. Remarkably, the asymptotic result of the telegraph model remains robust well outside the asymptotic limit. As a result, the approximations in the theory required to map it to the polymer model and solve it in the asymptotic limit are not the source of discrepancies between the predictions of the telegraph model and experimental distributions of the extensions of DNA during genome mapping. The agreement between theory and simulations motivates future work to determine the source of the remaining discrepancies between the predictions of the telegraph model and experimental distributions of the extensions of DNA in nanochannels used for genome mapping.

Published under license by AIP Publishing. <https://doi.org/10.1063/1.5109566>

I. INTRODUCTION

The problem of semiflexible polymers in channel confinement has received significant attention over the past decade owing to its application in the field of genome mapping,¹ where DNA molecules are confined in nanochannels to generate a coarse-grained map of the genome of interest. Theories^{2–5} and simulation techniques^{6–8} have matured to the point where clear demarcations between the four different regimes of confinement proposed by Odijk³ have been identified, and the relevant scaling theories for each regime have been confirmed by simulation.^{4,8,9}

Experimental conditions, however, rarely abide by the strict inequalities defining the limits of the scaling regimes.³ For example, for typical experimental conditions, the DNA persistence length is 50 nm and the effective width is 5 nm, whereupon the channel size would have to be around 5 nm to satisfy the condition $D \ll l_p$ for the Odijk regime. Conversely, the channel size needs to be much larger than 500 nm to be strictly in the de Gennes scaling regime ($D \gg l_p^2/w$). Hence, typical experiments involving confined DNA cannot be precisely described by either one of the scaling regimes.^{10–19}

Two recent publications have resolved this problem for channel sizes where the excluded volume effect is weak, which encompass most of the experimental parameter range. The first approach, proposed by Werner *et al.*,²⁰ uses a one-dimensional random walk model known as the weakly-correlated telegraph model. Dimensional analysis of this model furnishes a single scaling parameter, α , denoting the number of overlaps per hairpin in the DNA backbone, that collapses the data for both the fractional extension of the chain and the variance about that average extension onto master curves. The second approach, proposed by Chen,²¹ is a numerical solution of a self-consistent field theory (SCFT) for a channel-confined wormlike chain. SCFT also predicts that the extension of confined DNA can be explained by the same scaling parameter, and numerical solutions of the SCFT equations²¹ demonstrate the validity of the scaling parameter over an even wider parameter space than that identified by simulations of the telegraph model.²⁰

Recently in this journal, Ödman *et al.* developed a closed-form asymptotic solution to the telegraph model for the fractional extension distribution in channels close to the DNA persistence length, which is

the relevant regime for describing the physics of genome mapping.²² The comparison between experiments²³ and the theoretical predictions by Ödman *et al.*²² is suggestive but ultimately inconclusive. The key results from Ödman *et al.* are reproduced in Fig. 1. While both distributions have the same general form, with a heavy left tail due to the hairpin formation, the right tail of the theoretical distribution required fitting to the experimental data, rather than using the theoretical variance due to alignment fluctuations.^{24,25} Moreover, there were apparent discrepancies in the left tails of the distribution even after treating the channel size as an adjustable parameter to within a reasonable experimental error. Finally, it appears that the agreement between the theory and the experiment becomes worse as the channel size decreases. It is not apparent *a priori* whether the discrepancy between the asymptotic solution of the telegraph model²² and the experimental data²³ is due to a breakdown of the asymptotic theory caused by the experimental conditions, or whether the discrepancy lies elsewhere, for example in the use of a wormlike chain model to describe the experiments. It is also puzzling why the discrepancy is more pronounced for the smaller channels rather than the larger channels, since the larger channels are farther away from the asymptotic limit required by the theory.

To determine whether or not the asymptotic results for the telegraph model break down for these experimentally relevant conditions, we probed the extension distributions computationally, using pruned-enriched Rosenbluth method (PERM) simulations^{9,26} of confined wormlike chains. Our simulations encompass both the asymptotic limits for which the telegraph model solution has been derived,²² as well as experimentally relevant cases that do not satisfy the strict inequalities of the asymptotic limit. In order to capture the tails of the distribution, which exhibit extremely low frequencies, we have generated at least one million data points per case. These simulated distributions are compared with the theoretically predicted distributions without any adjustable parameters, revealing that the asymptotic theory is indeed robust, even when

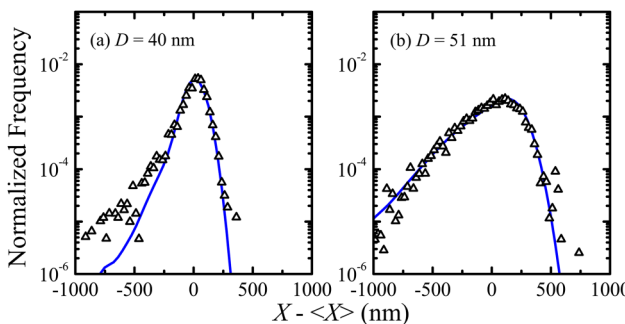


FIG. 1. Comparison between the asymptotic solution of the telegraph model for the distribution of the difference between the measured chain extension, X , and the average extension, $\langle X \rangle$, and experimental data made by Ödman *et al.*²² for the case of $L = 28\,125$ bp and (a) $D = 40$ nm ($D_{\text{eff}} = 36.4$ nm) and (b) $D = 51$ nm ($D_{\text{eff}} = 47.4$ nm). These correspond to the green curves in panels (a) and (c) in Fig. 3 of Ref. 22. Reproduced with permission from D. Ödman, E. Werner, K. D. Dorfman, C. Doering, and B. Mehlig, Biomicrofluidics **12**, 034115 (2018). Copyright 2018 AIP Publishing LLC.

the asymptotic conditions are only weakly satisfied. Furthermore, the quantification of the degree of agreement between the simulation and the theory using statistical parameters demonstrated that the theory only breaks down for small values of the scaling parameter, which correspond to channels much larger than those typically used in experiments.

II. THEORY

A wormlike chain confined in a nanochannel is characterized by multiple length scales: the polymer persistence length, l_p ,²⁷ the polymer effective width, w ,^{28,29} the polymer-wall depletion length, δ ,³⁰ and the effective channel size, $D_{\text{eff}} = D - \delta$, where D is the actual channel size. For a polyelectrolyte such as DNA, the persistence length,²⁷ effective width,^{28,29} and DNA-wall depletion length³⁰ are controlled by the intrinsic properties of the DNA, the wall chemistry, and the ionic strength of the solution, the latter governing the screening of electrostatic interactions. The relative values of these length scales dictate the extent to which the polymer stretches out to a fraction of its contour length, L , to produce a fractional extension, X/L .

Theories developed over the past 40 years provide predictions for the fractional extension of DNA^{2–5} for a given channel size and ionic strength. In the telegraph model of Werner *et al.*,²⁰ the DNA stretching problem was mapped to a one-dimensional correlated random walk. The relevant parameters of importance in this model are the average alignment of the DNA backbone with the channel axis, a , an excluded volume penalty for revisiting the same position along the channel axis, ϵ , and the rate of change of the direction of the walk, r . The latter quantity is inversely proportional to twice the global persistence length, g , which quantifies the typical distance between hairpin bends.³¹ From dimensional analysis, this trio of parameters can be combined into a single parameter, $\alpha = \epsilon g/a$, that represents the typical number of overlaps per hairpin bend. The parameter α alone determines the extension of the DNA molecule in this theory. The contour length, L , is equivalent to the total time, T , in the telegraph model. The mapping between the confined polymer parameters (D_{eff} , l_p , w) and the telegraph model parameters (a , g , ϵ) was computed by Werner *et al.*²⁰ via simulations of confined, ideal, wormlike chains.

In principle, one can compute the fractional extension distribution for long wormlike polymers directly from long-time simulations of the telegraph model for a given value of α . However, such simulations are prone to sampling errors and can become expensive if fine resolution is required as a function of the channel size. Fortunately, Ödman *et al.*²² solved the telegraph model in the limits of $\alpha \gg 1$ and $rT \gg 1$. Their analysis furnishes the fractional extension distribution

$$P_1(X', T) = \mathcal{N} \frac{1 + \sqrt{1 - X'^2}}{(1 - X'^2)^{3/4}} \exp[-rTS(X')], \quad (1)$$

where $X' = X/(aL)$ is the contour length projected onto the channel axis, \mathcal{N} is a normalization factor, and

$$S(X') = 3\alpha(1 - X') + 1 - \sqrt{1 - X'^2} \quad (2)$$

is the action.

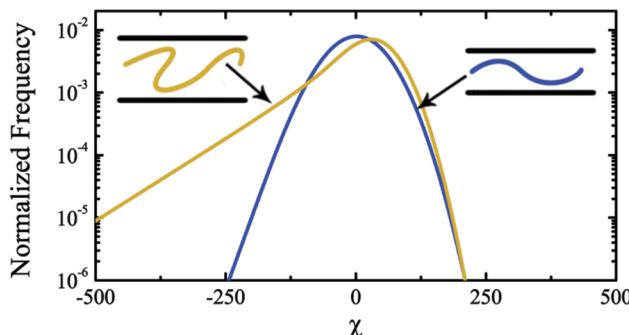


FIG. 2. DNA under a strong degree of confinement, $\alpha \gg 1$, stretch out to a substantial fraction of their contour length and produce a distribution that is approximately Gaussian (blue). As the degree of confinement is reduced, the DNA begins to form hairpins which bias the distribution to the smaller extension values leading to the left tail in the distribution (gold). The dimensionless extension, χ , is defined in Eq. (6).

The telegraph model only accounts for the effect of hairpin formation on the chain stretching. For the reasonably strong confinement $\alpha \gg 1$, the fluctuations about the average alignment a between the DNA backbone and the channel axis predicted by Odijk²⁴ become important and eventually dominate the variance in the chain extension.²⁰ The effect of these fluctuations, which are depicted schematically in Fig. 2, can be incorporated into the theory via the convolution integral²²

$$\mathcal{P}(X, L) = \int_0^{aL} P_1(X_1, L) \rho(X_1 - X) dX_1. \quad (3)$$

The function ρ is modeled as the Gaussian distribution that would be expected for small alignment fluctuations about the average orientation in the Odijk regime

$$\rho(\delta X) = (2\pi\sigma_0^2)^{-1/2} \exp\left[-\frac{\delta X^2}{2\sigma_0^2}\right], \quad (4)$$

where σ_0 is the variance in the chain extension in the absence of hairpins,^{24,25}

$$\sigma_0^2 = 0.00956 \frac{D_{\text{eff}}^2}{l_p} L. \quad (5)$$

III. METHODS

To construct distributions for the generalized problem of a polymer confined in a nanochannel, we first choose values of D_{eff} , l_p , and w which correspond to either (i) the asymptotic limits of the theory or (ii) the nonasymptotic cases that would be more typical of experiments. The corresponding telegraph model parameters a , r , and α were calculated from the polymer problem parameters by fitting to the curves in Werner *et al.*,²⁰ and σ_0 was computed from Eq. (5). The interpolation of the telegraph model parameters is accurate only in the range of $0.4 < D_{\text{eff}}/l_p < 24$, and additional ideal wormlike chain simulations would be required to calculate parameters outside that range. Table S1 in the supplementary material lists the sets of parameter values considered here.

The extension distributions predicted from the solution of the telegraph model were computed numerically by discretizing the convolution integral in Eq. (3). There are some subtleties in the accurate evaluation of Eq. (3), so it is worthwhile to provide a detailed explanation. The function $P_1(X')$ in Eq. (1) was first calculated over a range of $0 \leq X' < 1$ at intervals of 0.0001 and subsequently normalized by the area under the computed curve. The value of $\langle X \rangle$ for the resulting distribution was obtained by calculating the expected value of X' over this function, multiplied by rT . Subsequently, the convolution of $P_1(X')$ with $\rho(\delta X)$ in Eq. (3) was computed by defining a discrete scale for $X - \langle X \rangle$ followed by numerical integration. The value of σ_0 was calculated directly from Eq. (5). In contrast to previous work comparing the telegraph model to experiments,²² there are no adjustable parameters in the present analysis.

We also computed the extension distributions using pruned-enriched Rosenbluth method (PERM) simulations^{26,32,33} of a discrete wormlike chain model⁸ comprising N beads of diameter w and bond length b such that $L = Nb$ is the total contour length of the chain. In keeping with the cylindrical excluded volume interactions used in the previous analysis of the telegraph model,²⁰ we have used the ratio $w/b = 2$. As this choice of parameters leads to overlapping beads, we have not included the overlap penalty for contiguous trios of beads,^{34,35} but have retained the hard-core excluded volume penalty between all other bead pairs and between the beads and the walls. In the simulation, a single tour is executed by adding beads to the growing chain one bead at a time based on their Rosenbluth weights.³⁶ To avoid the attrition problem associated with the Rosenbluth-Rosenbluth method,³⁶ PERM^{26,32} also copies (enriches) configurations with high weights and destroys (prunes) configurations with low weights. For the enriching case, the statistical weight associated with the configuration that is being enriched is split between the two copies of that configuration. A tour is completed when all of these branches are either pruned or grow to the full contour length. This process is repeated for 100 000 tours. The simulations produce files containing the extension, X , and corresponding cumulative Rosenbluth weights for each chain from the branches that grew up to the full contour length. For convenience, we define

$$\chi = \frac{X - \langle X \rangle}{b} \quad (6)$$

as the dimensionless extension about the mean. Normalized histograms for χ were then plotted using MATLAB in each case. Relevant data from these histograms were extracted and plotted alongside the theoretical distributions for comparison.

To statistically quantify the deviations between theory and simulations, we performed a trio of statistical tests based on the cumulative distribution functions (CDFs) for χ , which are bounded between 0 and 1 and hence provide a uniform range for comparison. The simplest metric for the deviations is the root mean square error (RMSE) between the theoretical distributions, i.e., the CDF from the asymptotic solution of the telegraph model, $F(x)$, and the bins of the histograms from which the simulated distributions have been obtained.

We also obtained measures of this deviation using empirical distribution function (EDF) goodness of fit tests.³⁷ These are standard statistical tests typically used for assessing the normality of data samples but can be applied to determine if data have been drawn from any particular distribution. We have adopted their definitions to measure the distance between the empirical data distributions (from the PERM simulations) and the theoretical distributions (from the telegraph model). To perform this EDF test, the simulated values of fractional extensions for a given set of parameters, x_i ($i = 1, 2, \dots, n$) are sorted in an ascending order. The distance, ω , between the hypothesized cumulative distribution function, $F(x)$, and an empirical distribution function of the sample, $F_n(x)$, is given by

$$\omega^2 = \int_{-\infty}^{\infty} [F_n(x) - F(x)]^2 w(x) dF(x), \quad (7)$$

where the function $w(x)$ is a weighting function. Since the data for $F_n(x)$, which correspond here to the CDF for the PERM simulation data, are only known at discrete points, ω is evaluated by converting the integral in Eq. (7) into a sum of integrals.³⁸

The choice of weighting function $w(x)$ depends on which features of the distribution are important. When the weighting function is $w(x) = 1$, we are considering the deviations uniformly over the whole curve and the corresponding measure of deviation, ω_{CM} , is called the Cramér-von Mises criterion.³⁹ For one sample, the Cramér-von Mises criterion for Eq. (7) simplifies to³⁷

$$\omega_{CM}^2 = \frac{1}{n} \left\{ \sum_{i=1}^n \left(F(x_i) - \frac{(2i-1)}{2n} \right)^2 + \frac{1}{12n} \right\}. \quad (8)$$

For the Anderson-Darling criterion,^{38,40} ω_{AD} , the weighting function is $w(x) = 1/[F(x)(1-F(x))]$. This choice of $w(x)$ puts more emphasis on the tails of the distribution as opposed to the Cramér-von Mises criterion. This emphasis is imposed by the singularity of $w(x)$ in the tails of the distribution, which amplifies small errors therein. For one sample, the Anderson-Darling criterion for Eq. (7) simplifies to³⁷

$$\omega_{AD}^2 = \frac{1}{n} \left\{ - \sum_{i=1}^n \left(\frac{(2i-1)}{n} [\ln F(x_i) + \ln(1-F(x_{n+1-i}))] \right) - n \right\}. \quad (9)$$

IV. RESULTS AND DISCUSSION

To test the validity of the theory put forward by Ödman *et al.*²² describing the distributions of the fractional extension of confined DNA molecules, we first conducted PERM simulations³³ for five cases (1–5) at the asymptotic limits of the theory, where the theory is expected to be correct ($\alpha \gg 1$ and $rT \gg 1$) and for four nonasymptotic cases (N-1 to N-4) that do not satisfy the inequalities used by Ödman *et al.*²² to derive Eq. (3). These cases are tabulated in Table S1 in the supplementary material.

A. Illustrative examples

For the cases corresponding to the asymptotic limits of the theory, one would expect the simulation results to line up well with

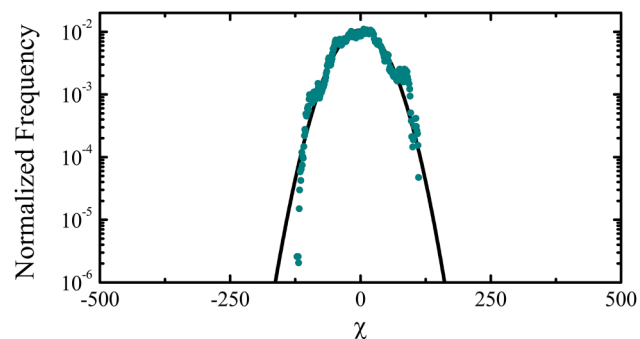


FIG. 3. Theoretical distribution (black curve) and simulated probability densities (cyan circles) for the parameters $\alpha = 29.1$ and $rT = 73.9$. This is case 2 in Table S1.

the theoretical predictions, since the assumptions made in the theory developed by Ödman *et al.*²² are valid in the limits of large α and large rT . The distributions were generated as detailed in Sec. III and indeed match. One such distribution for $\alpha \gg 1$ and $rT \gg 1$ is shown in Fig. 3, and the remaining cases are provided in the supplementary material. The discrepancies at the tails of the distributions are likely due to sampling errors that arise when simulating these highly confined chains; with 10^6 samples, we would expect significant errors at probabilities below 10^{-5} .

The cases for which the assumptions in the theory are not strictly satisfied are arguably more interesting. These cases align more closely with real experimental conditions. An example corresponding to a small DNA chain of contour length 5000 nm in a 50 nm channel at an ionic strength of 60 mM is shown in Fig. 4. This plot reveals that, even for a case not strictly satisfying the limits of $\alpha \gg 1$ and $rT \gg 1$, the simulated distributions agree with the theoretical predictions. Similar agreement was noted in the remaining distributions which are provided in the supplementary material. As noted in Sec. III, there are no adjustable parameters.

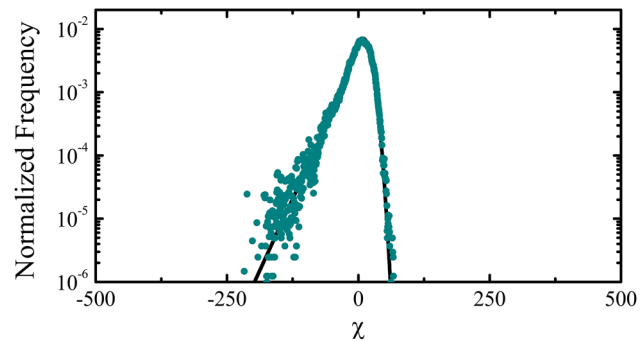


FIG. 4. Theoretical distributions (black curve) and simulated probability densities (cyan circles) for $\alpha = 3.81$ and $rT = 4.69$. This is case N-1 in Table S1.

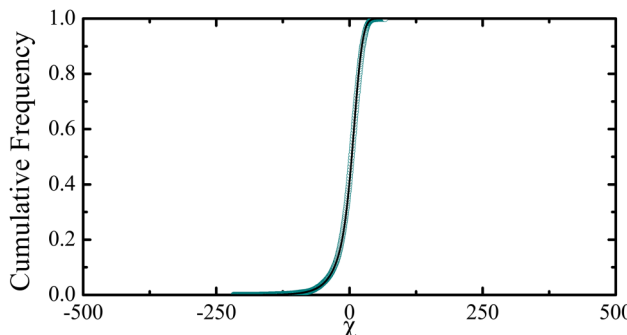


FIG. 5. The cumulative distribution functions corresponding to the probability distributions in Fig. 4. The difference between the theoretical distribution (black curve) and the simulated distribution (cyan circles) is used to quantify the degree of agreement.

B. Quantification of agreement and limits of the theory

Although the agreement between theory and simulation is qualitatively apparent in the cases described above and their counterparts in the [supplementary material](#), it is worthwhile to statistically quantify the degree of agreement by measuring the deviation between the theoretical and simulated distributions. To have a uniform range for comparison across the different cases, we have converted the probability distribution functions described previously into cumulative distribution functions. Figure 5 shows an example of the CDFs for both the theory and the simulation data in plots in Fig. 4.

The asymptotic theory for the distribution of label spacings, though expected to be valid only at the limits of $\alpha \gg 1$ and $rT \gg 1$, was found to hold even for values of α and rT not at these asymptotic limits. However, this does not imply that the theory is valid for all values of α and rT . To identify the limits of validity of the theoretical distributions, we performed simulations for nine

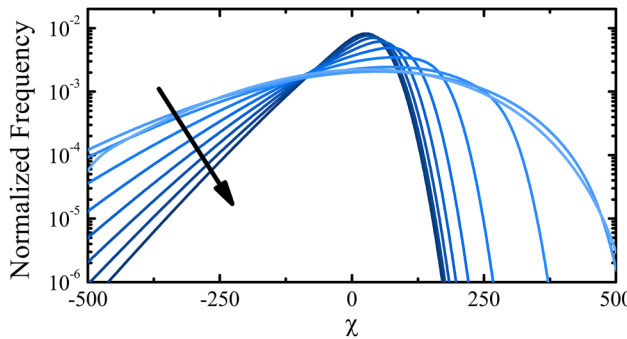


FIG. 6. Extension distributions predicted by the telegraph model for values of α between 0.2 and 3 at fixed $rT = 20$. The direction of the arrow and increased darkness of the lines correspond to increasing α .

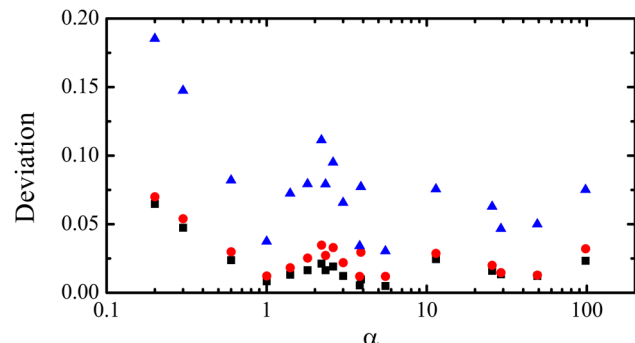


FIG. 7. Three statistical measures of deviation used to quantify the degree of agreement between the theoretical and simulated distributions: the root mean square error (black squares), the Cramér-von Mises statistic ω_{CM} (red circles), and the Anderson-Darling statistic, ω_{AD} (blue triangles).

additional cases at a constant value of $rT = 20$, which correspond to long chains and with values of α ranging from 0.2 to 3. The effect of this parameter sweep on the shape of the distributions can be seen in Fig. 6—the distributions get narrower as α increases. This narrowing is expected due to the reduction in both the Odijk variance due to alignment fluctuations and the suppression of hairpin formation. Indeed, for an infinitely large value of α , the distribution would approach a delta function. The details of these additional cases, as well as their probability and cumulative distribution functions, are provided in the [supplementary material](#).

The statistical measures of deviation described in Sec. III were computed for all the cases using the CDFs. The root mean square error was used to quantify the deviation between the theoretical and simulated distributions using the histogram bins of the simulated distributions, whereas the Cramér-von Mises criterion (ω_{CM}) and the Anderson-Darling criterion (ω_{AD}) used the continuous empirical distribution function without first binning the data. All of these measures of deviation are plotted against α in Fig. 7.

For higher values of α , all of the measures of deviation remain largely constant as a function of α . The sampling issues for small channels alluded to earlier are also apparent from the slight uptick in the deviations at $\alpha \approx 100$. The theory begins to break down only for small values of $\alpha \approx 0.3$, where there is a sudden rise in the statistical measures of deviation as α decreases. This qualitative effect can also be seen clearly in the individual distributions provided in the [supplementary material](#). Overall, however, the distributions predicted by the telegraph model are valid even when the asymptotic conditions forming the premises of the theory are not strictly satisfied.

V. CONCLUSION

We have shown that the asymptotic solution of the telegraph model by Ödman *et al.*²² provides a remarkably good description of simulation data for a confined wormlike chain, even for values of the parameters far from the asymptotic limit required by the theory. As a result, we can infer that the disagreement between the predictions of the telegraph model²² and experiments for DNA during genome

mapping²³ is not due to the fact that the experimental conditions do not strictly satisfy the inequalities in the theory.

However, the question still remains: what causes the disparity between experiments and theory? On the one hand, the analysis methods employed to generate the data in these experiments may introduce artifacts into the distributions. For example, most of these experiments require DNA molecules at least 150 kilobase pairs in length to be considered for analysis,^{23,30,41} and the alignment algorithm used for genomics applications might discard molecules which contain large hairpins that prevent alignment with the reference genome, thus affecting the left tail of the distribution. On the other hand, the omission of electrostatics when modeling the DNA as a wormlike chain interacting with a hard wall, which requires mapping the electrostatics to an equivalent neutral chain model, may cause the discrepancies. We anticipate that this study will direct further investigation into the experimental distributions using focused experiments and analysis of the underlying models to bridge this gap between experiments and theory.

SUPPLEMENTARY MATERIAL

See the [supplementary material](#) for (i) the parameters used for all of the cases in this paper and (ii) plots for the normalized frequency and the cumulative distribution function for each case.

ACKNOWLEDGMENTS

We thank Bernhard Mehlig and Daniel Ödman for discussions about their theoretical distributions and Guo Kang Cheong for discussions about PERM simulations. This work was supported by the National Institutes of Health (NIH) (No. R01-HG006851). Computational resources were provided in part by the Minnesota Supercomputing Institute.

REFERENCES

- ¹E. T. Lam, A. Hastie, C. Lin, D. Ehrlich, S. K. Das, M. D. Austin, P. Deshpande, H. Cao, N. Nagarajan, M. Xiao, and P.-Y. Kwok, *Nat. Biotechnol.* **30**, 771 (2012).
- ²M. Daoud and P. G. de Gennes, *J. Phys.* **38**, 85 (1977).
- ³T. Odijk, *Phys. Rev. E* **77**, 060901 (2008).
- ⁴E. Werner and B. Mehlig, *Phys. Rev. E* **90**, 062602 (2014).
- ⁵L. Dai, J. R. C. van der Maarel, and P. S. Doyle, *Macromolecules* **47**, 2445 (2014).
- ⁶P. Cifra, Z. Benková, and T. Bleha, *J. Phys. Chem. B* **113**, 1843 (2009).
- ⁷P. Cifra, *J. Chem. Phys.* **131**, 224903 (2009).
- ⁸Y. Wang, D. R. Tree, and K. D. Dorfman, *Macromolecules* **44**, 6594 (2011).
- ⁹A. Muralidhar, D. R. Tree, and K. D. Dorfman, *Macromolecules* **47**, 8446 (2014).
- ¹⁰W. Reisner, K. J. Morton, R. Riehn, Y. M. Wang, Z. Yu, M. Rosen, J. C. Sturm, S. Y. Chou, E. Frey, and R. H. Austin, *Phys. Rev. Lett.* **94**, 196101 (2005).
- ¹¹W. Reisner, J. P. Beech, N. B. Larsen, H. Flyvbjerg, A. Kristensen, and J. O. Tegenfeldt, *Phys. Rev. Lett.* **99**, 058302 (2007).
- ¹²C.-C. Hsieh, A. Baldacci, and P. S. Doyle, *Nano Lett.* **8**, 1683 (2008).
- ¹³C. Zhang, F. Zhang, J. A. van Kan, and J. R. C. van der Maarel, *J. Chem. Phys.* **128**, 225109 (2008).
- ¹⁴Y. Kim, K. S. Kim, K. L. Kounovsky, R. Chang, G. Y. Jung, J. J. de Pablo, K. Jo, and D. C. Schwartz, *Lab Chip* **11**, 1721 (2011).
- ¹⁵D. Gupta, J. J. Miller, A. Muralidhar, S. Mahshid, W. Reisner, and K. D. Dorfman, *ACS Macro Lett.* **4**, 759 (2015).
- ¹⁶S. Lee, Y. Lee, Y. Kim, C. Wang, J. Park, G. Jung, Y. Chen, R. Chang, S. Ikeda, H. Sugiyama *et al.*, *Polymers* **11**, 15 (2019).
- ¹⁷V. Iarko, E. Werner, L. Nyberg, V. Müller, J. Fritzsche, T. Ambjörnsson, J. Beech, J. Tegenfeldt, K. Mehlig, F. Westerlund, and B. Mehlig, *Phys. Rev. E* **92**, 062701 (2015).
- ¹⁸D. Gupta, J. Sheats, A. Muralidhar, J. J. Miller, D. E. Huang, S. Mahshid, K. D. Dorfman, and W. Reisner, *J. Chem. Phys.* **140**, 214901 (2014).
- ¹⁹D. Gupta, A. B. Bhandari, and K. D. Dorfman, *Macromolecules* **51**, 1748 (2018).
- ²⁰E. Werner, G. K. Cheong, D. Gupta, K. D. Dorfman, and B. Mehlig, *Phys. Rev. Lett.* **119**, 268102 (2017).
- ²¹J. Z. Y. Chen, *Phys. Rev. Lett.* **121**, 037801 (2018).
- ²²D. Ödman, E. Werner, K. D. Dorfman, C. Doering, and B. Mehlig, *Biomicrofluidics* **12**, 034115 (2018).
- ²³W. F. Reinhart, J. G. Reifenberger, D. Gupta, A. Muralidhar, J. Sheats, H. Cao, and K. D. Dorfman, *J. Chem. Phys.* **142**, 064902 (2015).
- ²⁴T. Odijk, *Macromolecules* **16**, 1340 (1983).
- ²⁵T. W. Burkhardt, Y. Yang, and G. Gompper, *Phys. Rev. E* **82**, 041801 (2010).
- ²⁶T. Prellberg and J. Krawczyk, *Phys. Rev. Lett.* **92**, 120602 (2004).
- ²⁷A. V. Dobrynin, *Macromolecules* **38**, 9304 (2005).
- ²⁸D. Stigter, *J. Colloid Interface Sci.* **53**, 296 (1975).
- ²⁹D. Stigter, *Biopolymers* **16**, 1435 (1977).
- ³⁰A. B. Bhandari, J. G. Reifenberger, H.-M. Chuang, H. Cao, and K. D. Dorfman, *J. Chem. Phys.* **149**, 104901 (2018).
- ³¹T. Odijk, *J. Chem. Phys.* **125**, 204904 (2006).
- ³²P. Grassberger, *Phys. Rev. E* **56**, 3682 (1997).
- ³³D. R. Tree, A. Muralidhar, P. S. Doyle, and K. D. Dorfman, *Macromolecules* **46**, 8369 (2013).
- ³⁴A. Muralidhar and K. D. Dorfman, *Macromolecules* **48**, 2829 (2015).
- ³⁵K. D. Dorfman, *J. Biomech. Eng.* **140**, 020801 (2018).
- ³⁶M. N. Rosenbluth and A. W. Rosenbluth, *J. Chem. Phys.* **23**, 356 (1955).
- ³⁷M. A. Stephens, *J. Am. Stat. Assoc.* **69**, 730 (1974).
- ³⁸T. W. Anderson and D. A. Darling, *J. Am. Stat. Assoc.* **49**, 765 (1954).
- ³⁹H. Cramér, *Scand. Actuar. J.* **1928**, 13 (1928).
- ⁴⁰T. W. Anderson, D. A. Darling *et al.*, *Ann. Math. Stat.* **23**, 193 (1952).
- ⁴¹H.-M. Chuang, J. G. Reifenberger, H. Cao, and K. D. Dorfman, *Phys. Rev. Lett.* **119**, 227802 (2017).